PCCP

Accepted Manuscript

ROYAL SOCIETY OF CHEMISTRY

www.rsc.org/pccp

Physical Chemistry Chemical Physics RSCPublishing

ARTICLE

Evolution of Water Sorption in Catalyst Coated Membranes Subjected to Combined Chemical and Mechanical Degradation

Cite this: DOI: 10.1039/xoxxoooooox

Received ooth January 2012,
Accepted ooth January 2012

DOI: 10.1039/xoxxoooooox

www.rsc.org/

Senthil Velan Venkatesan,[a] Chan Lim,[a] Erin Rogers,[b] Steven Holdcroft,[c] and Erik Kjeang [a]

Catalyst coated perfluorosulfonic acid ionomer membranes (CCMs) were subjected to a combined chemical/mechanical accelerated stress test (AST) designed for rapid benchmarking of in-situ membrane stability in polymer electrolyte fuel cells. In order to understand the evolution of the ionomer water sorption characteristics during combined chemical/mechanical degradation, CCM samples were periodically extracted from the AST and analyzed for ionomer mass fraction and water sorption properties. In spite of severe fluoride release and membrane thinning, the water uptake per unit mass of the partially degraded CCMs was found to be essentially constant. The mass fraction of ionomer in the CCM samples determined from thermogravimetric analysis (TGA) showed significant material loss throughout the AST process due to ionomer degradation and fluoride release, up to roughly 50% at end-of-life. The effects proceeding at different stages of degradation were therefore more accurately revealed by ionomer mass-normalized data. The water uptake per unit gram of ionomer was shown to increase significantly with degradation, in contrast to the previous results normalized by CCM dry mass. Although increased water sorption may indicate enlarged solvated hydrophilic domains in the membrane, which would be beneficial for enhanced proton mobility, the proton conductivity was found to decrease. This finding suggests that the additional water sorbed in the membrane was not contributing to proton conduction and was therefore likely situated in non-ionic cavities formed through degradation rather than in the ionic clusters.

1. Introduction

The proton exchange membrane, also known as the polymer electrolyte membrane, is a key component in polymer electrolyte fuel cells which acts as an ion-conducting conduit while physically and electronically separating the anodic and cathodic half-cells. The membrane coated on both sides with catalyst layers constitutes a catalyst coated membrane (CCM), which is the principal power generating component in the membrane electrode assembly (MEA) of the fuel cell[1,2]. Water is essential for ion transport in the CCM. Proton conduction in the membrane depends on the internal water content and it is important to optimize the water content for efficient operation of fuel cells. The most commonly used fuel cell membrane is made of perfluorosulfonic acid (PFSA) ionomer which provides good chemical and mechanical stability. The PFSA ionomer molecular structure consists of branched hydrophilic sulfonic side chains attached to hydrophobic fluorocarbon main chain. When hydrated, it separates to hydrophilic clusters holding maximum water in the cavity for enhanced proton conduction mainly through vehicular and Grotthuss mechanisms. Water is constantly introduced into the fuel cell by reactant humidification and also produced as a by-product of the oxygen reduction reaction at the cathode. However, the generated water alone is not sufficient to hydrate the membrane for sustainable performance.

The sorption and diffusion of water in the ionomer phase determines the distribution of water in the CCM and in turn affects the local proton conductivity. A non-uniform water distribution in the membrane is caused by fluctuations in the current drawn from the fuel cell and inlet humidity of the reactants. There are many practices adopted in literature to maintain uniform hydration of fuel cells: for example, by introducing additives in the membrane[3,4] or catalyst layer[5], or modifying the structure of the gas diffusion layer[6,7]. The mechanism for water sorption and desorption in simple form was reported by Majsztrik et al.[8]. The water uptake in PFSA membranes is believed to occur by adsorption of water on the walls of the hydrophilic domains followed by dissolution of

sulfonic acid end groups with an increase in the water content, and further increase in bulk water volume with increasing humidity[8]. The process of absorption from the vapor phase commences with the transport of water across the gas/membrane interface and then into the membrane. Further, the vapor reaches the interior of the membrane through diffusion, followed by swelling to accommodate free water in the hydrophilic regions surrounded by SO_3^- groups. Desorption takes place through diffusion from the interior to the gas/membrane interface and from the interface to the gas phase[8]. The water sorption of PFSA membranes was published in a number of articles considering the water transport across the gas/membrane interface and through the bulk membrane[9-11], but the mechanism of water sorption in a CCM also includes the transport of water across the gas/ionomer interface in catalyst layers. The states (polarized and un-polarized) of water in the hydrophilic pore determine the amount of water that can be accommodated and in turn determine the water uptake and transport properties of the membrane in the CCM[12]. The microstructure of the membrane is strongly linked to the water uptake and water dynamics[13-15]. The membrane water uptake during fuel cell operation is an important factor in the conjoined fuel cell performance and membrane durability, and hence an important factor in the design of fuel cell MEAs.

Membranes are exposed to mechanical, thermal, and chemical stressors during fuel cell operation. The change in morphology and molecular structure of the ionomer membrane with chemical degradation was experimentally investigated by atomic force microscopy (AFM)[16], nuclear magnetic resonance (NMR)[17], and Fourier-transform infrared (FT-IR) techniques[18,19]. NMR revealed that the hydroxyl radicals (OH●), generated within the MEA, preferentially attack the α-O-CF_2 bond on the ionomer side chain, and that the radical attack further escalates via side chain unzipping towards the main chain with prolonged exposure[17]. A recent modeling study revealed the evolution of ionomer molecular structure and demonstrated the changes in physicochemical membrane properties with chemical degradation. The modeling analysis supports a proposed chemical degradation mechanism that is initiated by side chain cleavage, which is propagated through main chain scission and fragmentation[20,21]. In addition to the chemical stress, mechanical stress is known to cause substantial membrane degradation in the form of a fatigue-fracture process[22,23]. Variations in load and humidity levels expand and shrink the hydrophilic clusters in the ionomer membrane and thus induce a repetitive mechanical stress that can generate tears in the membrane upon prolonged exposure. It was recently demonstrated that the rate of mechanical degradation is exacerbated by chemical degradation[24,25]. The application of combined chemical and mechanical membrane degradation in a specialized accelerated stress test (AST) indicated a reduced time-to-failure compared to a purely chemical AST, which was attributed to the loss in membrane fracture strength induced by chemical degradation[26]. It is noteworthy that both chemical and mechanical degradation are known to occur during field operation of fuel cells; consequently, joint analysis of chemical and mechanical membrane stressors is essential.

Water uptake measurements of pristine and ex-situ chemically degraded PFSA membranes were recently reported in a few publications. Ghassemzadeh et al.[27] reported a decrease in the water uptake of a Nafion 211 membrane upon exposing it to hydroxyl radicals generated by e-beam irradiation of aqueous solutions of H_2O_2 and H_2SO_4. The decrease in water uptake was attributed to a reduction in the ion exchange capacity (IEC) values of the membrane and the resultant molecular structure of the constituent ionomer. Water uptake measurements of membranes that were degraded in Fenton's reagent were also reported. The ex-situ Fenton's Reagent test is highly aggressive in terms of very high ferrous ion and peroxide concentrations. Hence, degradation under such extreme conditions leads to rapid hydrogen peroxide decomposition which creates internal micropores in the membrane, i.e., 'blisters', which may increase the water uptake of the membrane simply by retaining bulk water in its cavities[28]. This is an artifact introduced by the ex-situ Fenton's Reagent test, which is not observed during in-situ membrane degradation in the fuel cell environment.

The water uptake of a CCM or MEA is less frequently reported in the literature. The CCM in a fuel cell is a composite material consisting of hygroscopic active ionomer in dispersed form and less hygroscopic carbon, Pt, and traces of PTFE in catalyst layers on both sides. The catalyst layers on both sides were shown to affect the mechanical[29] and swelling[30,31] properties of the membrane. Furthermore, the membrane behaves differently in terms of humidity cycling and water sorption when situated in the MEA[30]. The water transport through the membrane/electrode interface, diffusion of water in the membrane, and desorption of water through another membrane/electrode interface depends on the mass-transport coefficients for absorption/desorption and the diffusion coefficient of water. These kinetic properties are in turn dependent on the water content of the membrane in the MEA[32]. Apart from the ionomer water uptake, the capillarity of the catalyst layers could also play a role in the water sorption of the CCM. The CCM consists of at least two types of ionomer, which are chemically identical, but have different environments, i.e., ionomer in membrane form and dispersed ionomer in catalyst layers. The hydrophilic domain sizes in the two ionomer forms are different[33,34]. The distribution of water across the CCM has been explored previously using a soft x-ray scanning transmission x-ray microscope[35]. The membrane in the CCM had the highest and most uniform water content, followed by lesser water content in the catalyst layers. The catalyst layer portion farthest from the membrane, but in close proximity to the micro porous layer (MPL), had the least water content because of its partly hydrophobic nature[35,36].

With all the above factors taken into consideration, part of our motivation is to bridge the existing gap in the literature between previous water uptake studies and the in-situ membrane degradation in the CCM. The overall objective of the present work is therefore to determine the effect of coupled

chemical and mechanical degradation stressors on the water uptake behavior and thermal stability of in-situ degraded catalyst coated membranes. The proposed structure-property analysis of in-situ degraded CCMs is intended to shed new light on the complex interactions between the internal degradation stressors and the overall durability of the fuel cell stack, which is essential for the ongoing growth in commercialization of reliable PEFC technologies for both automotive and stationary power applications.

2. Experimental

2.1. In-situ degradation protocol

A commercial PFSA-cast membrane in the protonic form was used in this work. Fuel cell stacks with MEAs fabricated from the same PFSA material by a proprietary method were supplied by Ballard Power Systems, Burnaby, BC. In order to evaluate the effects of combined chemical/mechanical stressors on the durability of the membrane, an in-situ cyclic open circuit voltage accelerated stress test (COCV AST) was applied. The COCV AST exposed the membrane/MEA to periodic chemical and mechanical stresses through open circuit voltage hold at high temperature, elevated oxygen concentration, and low relative humidity and alternating wet/dry operation until membrane failure occurred. Further information on the fuel cell assembly, COCV AST protocol, and a complete set of in-situ and ex-situ measurements can be found in our previously published article by Lim et al.[25]. Partially degraded CCM samples were extracted from the AST stacks at different numbers of cycles. A hydrogen leak rate indicative of stack failure was observed after 13 cycles which represents the end-of-life (EOL) of the stack.

2.2. In-situ diagnostic methods

Previously, Lim et al.[25] reported the state of health of the fuel cell membrane during COCV AST using in-situ techniques such as high frequency resistance (HFR) monitoring, OCV decay, electrochemical leak detection test (ELDT), and fluoride emission rate (FER) measurements. In the present work, the HFR values recorded at 1 kHz were adopted from Lim et al.[25] to calculate the change in proton conductivity due to combined chemical and mechanical membrane degradation. The HFR of the reference cell was subtracted from the obtained HFR values to accurately quantify the resistance change of the ionomer induced by degradation. The proton conductivity was calculated based on the following relation:

$$\sigma = \frac{l}{Z \times A} \qquad \text{Equation (1)}$$

where l is the normalized thickness of the membrane, Z is the high frequency resistance, and A is the electrode area of the CCM, in SI units. The outlet effluent water from the anode and cathode half-cells was sent through inline fluoride concentration meters to monitor the fluoride emission rates during the AST.

2.3. Ex-situ characterization

The beginning-of-life (BOL) CCM and CCMs extracted after the 0^{th}, 2^{nd}, 5^{th}, 8^{th}, 11^{th}, and 13^{th} cycle of the COCV AST operation were characterized using ex-situ techniques for water uptake, ionomer mass fraction, and membrane thickness. The degraded CCMs were delaminated from the MEAs and cut into fine pieces. The water uptake of the membrane and CCM samples were studied using a multi-vapor gravimetric sorption analyzer (Surface Measurement System Ltd.). A known mass of pristine membrane, BOL, partially degraded, and EOL CCM samples were packed in a stainless steel mesh sample pan. During the experiments, nitrogen purge gas was flown at a rate of 200 sccm. After loading the sample, sufficient time (~270 min) was allowed to reach the steady state before starting the experiments. Once the steady state was reached, the relative humidity (RH) was increased from 0 to 100% and decreased back to 0% in steps of 10%, while sufficient time (~120 min) was allowed to reach sample equilibrium at each step. The mass of the sample was monitored with a high precision microbalance with an accuracy of 0.1 µg. The absorption and desorption isotherms were obtained with increasing and decreasing RH, respectively. The water uptake of the sample was calculated as follows:

$$Water\ uptake,\ \% = \frac{(W_{100} - W_0)}{W_0} \times 100 \qquad \text{Equation (2)}$$

where, W_{100} and W_0 are the sample mass in gram measured at 100% and 0% RH, respectively.

Thermogravimetric analysis (TGA) of the membrane and CCM samples was carried out using a Pyris 1 TGA instrument (Perkin Elmer) to measure the mass fraction of ionomer in each sample and monitor the thermal stability of the materials at different levels of degradation. The samples were heated from 25°C to 750°C at a heating rate of 5°C min^{-1}. Dry nitrogen gas was used to create a protective gas sheath to prevent oxidation of the sample by air at high temperature. A high precision microbalance from Ohaus with a readability of 0.1 mg was used to measure the mass of the membrane and CCM samples with known areal dimensions at ambient conditions. The membrane thickness was measured from cross-sectional MEA images obtained with a Philips XL30 scanning electron microscope (SEM) and used in the proton conductivity calculations (cf., Equation 1).

3. Results and discussion

The present work deals with understanding the water uptake behavior of catalyst coated fuel cell membranes (CCM) subjected to combined chemical and mechanical degradation. The effects of membrane degradation on the water uptake and thermal stability of the CCM were evaluated and presented as follows. The results from the multi-vapor gravimetric sorption analyzer were used to interpret the dynamics of water and its correlation to the membrane degradation. The thermal stability and mass fraction of the ionomer present in the CCM were

evaluated using thermal analysis. These results were also used in the normalization of the water sorption by ionomer mass of the degraded materials. The experimental analysis was also extended to explore changes in proton conductivity calculated from the in-situ high frequency resistance and fluoride emission rates caused by membrane degradation.

3.1. Water uptake

The ionomer membrane water uptake is an important factor in deciding the performance of polymer electrolyte fuel cells; and for the same reason, this subject has been widely investigated on pristine membranes. In the present work, the water uptake of pristine membrane, BOL CCM, and COCV AST degraded CCMs was analyzed. Pristine membranes are known to exhibit distinctive regions in the absorption and desorption curves[8]. Different regions are designated as follows: initial absorption from the vapor phase (0-10% RH); slow addition of water through diffusion (10-80% RH); followed by swelling to accommodate free water (>80% RH). Desorption takes place through diffusion from the interior to the gas/membrane interface and from the interface to the gas phase. In the water uptake process, the membrane is forced to swell during absorption and contract back toward the original state after complete desorption[8], though a small amount of hysteresis generally remains in the material. Hence, as shown in Fig. 1, the obtained water sorption and desorption curves were asymmetric for the same membrane sample. The BOL CCM showed similar behavior to that of the membrane during the water sorption experiment, although the amount of water absorbed per mass unit of sample was lower than for the pure membrane. The water uptake of the BOL CCM was repeated three times to get the average and found to be within the variation range of ±0.3 wt.%. The variation could be attributed to the difference in the catalyst layer mass while peeling-off the diffusion media from the CCM. From the obtained results, the water content of the CCM was lower during absorption than during desorption at a given RH and the difference was more pronounced in the range of 55-100% RH. Beyond 55% RH, the water sorption of the pure membrane occurred steeply, whereas the CCM samples exhibited a more gradual increment. The lower water absorption of the CCM samples per unit mass could be substantiated due to the mass contribution from the catalyst layers. The constraint imposed on both sides of the membrane by the catalyst layers could impose more restrictive pathways for the interfacial transfer of vapor. Water transport across the membrane/catalyst layer interface and through the bulk membrane has to occur through one more barrier made of the gas/catalyst layer-ionomer interface. Above 80% RH, the water uptake per 10% rise in RH for the CCM was much less than for the membrane, which could be attributed to reduced membrane sorption and expansion due to the confinement provided by the catalyst layers. This is in fair agreement with a recent report by Goulet et al.[30] which indicates the difference in expansion and contraction behavior of pristine membranes and membranes confined in CCMs and MEAs.

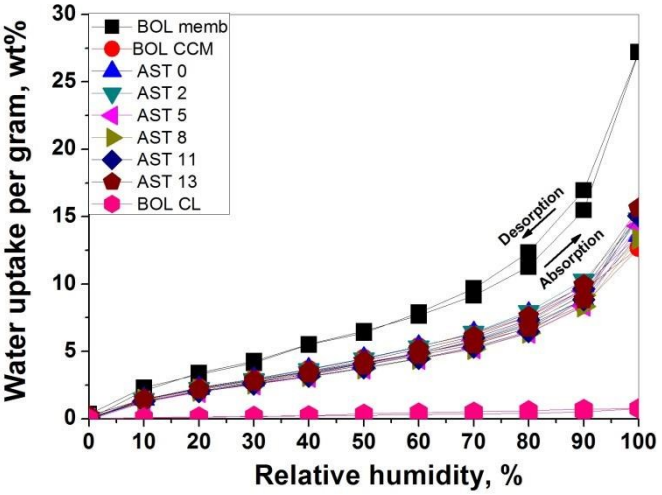

Fig. 1 Water sorption isotherms of pristine membrane, catalyst layer, BOL CCM, and degraded CCMs extracted after various numbers of COCV AST cycles (as indicated).

Measurements on the degraded CCM samples representing the 2nd, 5th, 8th, and 11th AST cycle and EOL were also carried out and the corresponding water uptake isotherms are presented in Fig. 1. At a first glance, the results obtained for the degraded CCMs appear quite similar to the results for the BOL CCM. The water uptake of the CCM samples calculated at 100% RH is also presented in Fig. 2 to further analyze the water sorption of the degraded CCMs at the fully hydrated state. The water uptake of the pristine membrane used in this study was found to be 27.5 wt.% at 100% RH, while the corresponding water uptake of the CCMs was in the 12-16 wt.% range. Since the CCM material is a composite structure, the mass contribution from Pt/C and the porous nature of the catalyst layers must also be considered in the water sorption calculations. To precisely investigate the effects of capillarity and absorption by the distributed ionomer in the anode and cathode catalyst layers on the overall water sorption behavior of the catalyst coated membrane, a control experiment was conducted on pure catalyst layers by separating them from the BOL CCM (cf., BOL CL in Fig. 1). It is observed that the carbon supported catalyst powder and ionomer in the dispersed form did not absorb more than 0.8 wt.% of water. This could be due to the lesser amount of ionomer and smaller dimension of hydrophilic domains in the catalyst layer ionomer relative to the bulk membrane. The ionomer in the catalyst layer exists in the form of a thin film and agglomerated lumps in and around the catalyst nanoparticles. A detailed review on the nature of the ionomer and its interaction with Pt and carbon in the catalyst layer can be found elsewhere[33]. The nanoparticles of platinum on hydrophobic carbon support could adsorb water, but merely a negligible amount compared to the ionomer phase in the CCM. We can thus infer that the water uptake contribution of the CCM samples primarily comes from the membrane ionomer phase and only a small amount is contributed from the catalyst layer.

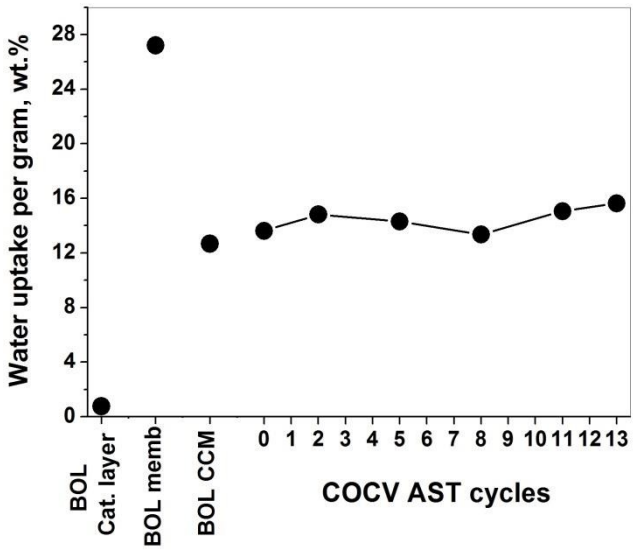

Fig. 2 Gravimetric water uptake of pristine catalyst layer, membrane, CCM (average of three experiments with ±0.3 wt.% standard deviation), and AST degraded CCMs at 100% RH.

After conditioning of the CCM, the water uptake increased as the membrane in the CCM sample was sufficiently hydrated and internal water channels were formed. The increase in water uptake continued during the first two cycles of the COCV AST experiment as the conditioning effect appeared to dominate over the relatively mild membrane degradation at this stage. With substantial chemical degradation in subsequent AST cycles, however, a considerable reduction in water uptake was observed until the 8th cycle due to the loss of sulfonic acid end groups and associated water. On the contrary, the highest level of water uptake was obtained for the EOL CCM, potentially due to the physical damage in the membrane caused by the mechanical stress that acted on the chemically weakened ionomer structure at more advanced stages of degradation.

As significant membrane thinning was observed with COCV AST cycles, the water uptake results could be masked by the reduction in the mass and volume of the ionomer membrane. The areal water uptake was therefore measured and analyzed by normalizing the water uptake by the sample area taken for the DVS test, which is the only sample descriptive metric that was not altered by the membrane degradation process. As shown by the results in Fig. 3, the pure membrane contained the highest amount of water per unit area of sample. The BOL CCM absorbed less water per unit area due to the presence and confinement of the catalyst layers, as discussed previously. The reorientation of ionic clusters and formation of water channels during conditioning led to increased water sorption per unit area of CCM. The growth of hydrophilic domains continued somewhat until the 2nd AST cycle, followed by an extended period of decay in water uptake until the 11th cycle, indicative of chemical membrane degradation. With severe degradation, this trend was reversed, and the water uptake increased substantially in the final two AST cycles until EOL due to bulk water in newly formed membrane cavities induced by combined chemical/mechanical degradation. This trend can be correlated to the rapid growth in hydrogen leak rate across the membrane/CCM at the final stages of membrane degradation due to propagation of cracks and holes that support convective hydrogen crossover approaching leak induced MEA failure[25].

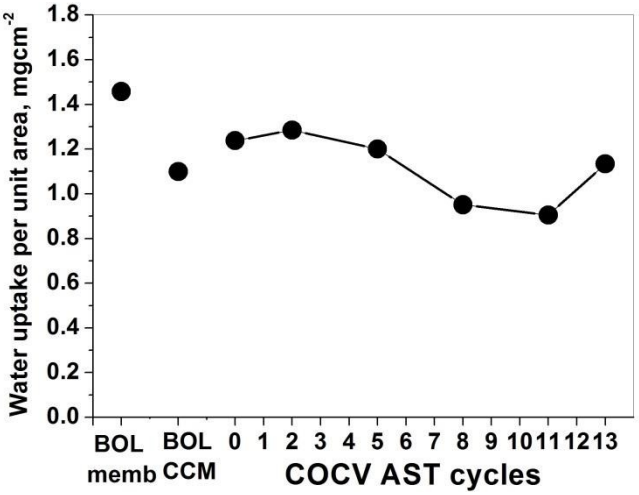

Fig. 3 Water uptake per unit area of pristine membrane, CCM, and AST degraded CCMs at 100 % RH.

3.2. Thermogravimetric analysis

The CCM is a composite material which consists of ionomer and catalyst particles. The compositional analysis of the different phases in such material is obtained through monitoring the mass loss by heating the material in a controlled atmosphere[30,37]. In order to understand the effect of ionomer degradation on the water sorption behavior of the membrane, it is necessary to separate the water sorption contribution of the ionomer in the CCM. Moreover, the thickness of the membrane decreased significantly during COCV AST operation, and the loss of ionomer material can mask any water uptake variation which occurs due to ionomer degradation. The dry PFSA ionomer content in the membrane and catalyst coated membranes was therefore determined using thermogravimetric analysis (TGA) by pyrolysis in a nitrogen atmosphere to thermally decompose the material. The nitrogen atmosphere was used to avoid combustion of carbon in the catalyst layers. The first derivative mass loss and thermogravimetric plots of pristine membrane, BOL, and EOL CCMs are shown in Fig. 4. Though TGA experiments were carried out on the dry membrane and CCM at higher temperatures than the actual operating temperature of PEFCs, high temperatures are considered as an external thermal stimulus to evaluate the decomposition patterns as a result of accelerated (chemical and mechanical) stressors. The thermal decomposition of the ionomer occurred at different stages. The widely accepted thermal decomposition products of PFSA ionomer are H_2O and SO_2 during the desulfonation process, and fluorinated small molecules as a result of chain scission during main chain decomposition events[4].

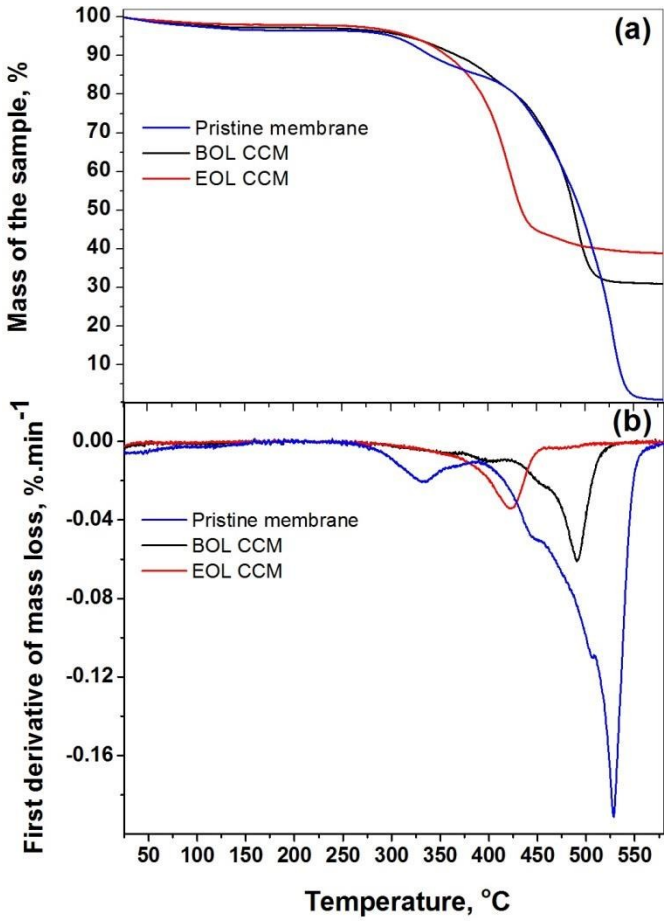

Fig. 4 (a) Thermogravimetric and (b) derivative thermogravimetric plots obtained for pristine membrane, BOL, and EOL CCM.

To resolve the overlapping processes conveniently, the temperature ramp rate was maintained at 5°C min^{-1}. PFSA ionomer is highly hydrophilic and sulfonic acid end groups hold water molecules until the desulfonation temperature of ~288°C. The mass difference between the desulfonation (~288°C) and complete ionomer decomposition (~560°C) temperature was assigned to the mass of dry ionomer present in the sample[38]. In case of the CCM, the remaining mass after complete decomposition of the ionomer was due to catalyst and carbon support particles that were not decomposed in the applied temperature range. The TGA scans recorded for the BOL CCM were similar to those observed for the pure membrane (Fig. 4a). The small initial mass loss in the 1st stage while heating to ~288°C is attributed to the loss of absorbed water molecules above which the desulfonation of the end group through the decomposition of C-S bond takes place until ~400°C in the 2nd stage. The mass loss in the 3rd stage of the decomposition represents the amount of ionomer lost due to side chain decay. The mass loss in the 4th stage of decomposition due to main chain decay overlaps with the 3rd stage in the temperature range of 370-560°C[38]. The rate of change of mass with temperature distinguishes the onset and completion of the decomposition events in the first derivative thermogravimetric (DTG) plot (Fig. 4b). The pristine membrane decomposed at a marginally higher temperature than the ionomer in the CCM, which indicates that the pristine membrane had better stability towards thermal decomposition than the CCM. The presence of signal between 300-350°C for the pristine membrane could be due to removal of moisture and sulfonic end group decomposition[39]. The side chain and main chain decomposition occurred after 350°C in both membranes and CCMs. The presence of platinum in the CCM catalyzes the thermal decomposition of the polytetrafluoroethylene (PTFE) like backbone in the ionomer at high temperatures[39]. In addition to the effect of platinum, the degradation history of the EOL CCM is shown to bring the mass loss events further to a lower temperature than the BOL CCM mass loss events. The side chain and main chain decomposition processes also take place at lower temperatures for the degraded membrane. This could be ascribed to the changes in the molecular structure of the PFSA ionomer caused by chemical membrane degradation. The BOL CCM is thermally more stable than the EOL CCM in terms of the precedence of the degradation events. The reduced thermal stability of the EOL CCM can be correlated with the decay in mechanical properties observed previously[24-26] due to the unbalanced intermolecular attraction between the hydrophilic and hydrophobic phases created by the ionomer degradation. The same reason could be attributed for the reduced mechanical strength of the membrane observed experimentally by Sadeghi Alavijeh et al.[26].

The mass loss that occurs per unit area of the CCM could potentially be used to track the magnitude of chemical membrane degradation during fuel cell operation, similar to a fluoride release measurement. The areal mass of the COCV AST degraded CCMs was measured from a microbalance (Fig. 5a), while the mass fraction of dry ionomer in the CCMs was determined from TGA (Fig. 5b). The measured ionomer mass fraction of the CCM was found to decrease linearly with the COCV AST cycles (Fig. 5b). This is the collective amount of ionomer in the membrane and dispersed form in the catalyst layer. Due to the high level of chemical stress induced by the COCV AST, both forms of ionomer are expected to undergo degradation, and it is difficult to accurately measure and distinguish them in an in-situ experiment. At EOL, the CCM had lost ~46 wt.% of the ionomer due to the advanced stage of chemical degradation, known to progress through side chain cleavage and propagate through main chain unzipping and fragmentation[17,20,21]. The ionomer material loss measured from thermal analysis can be correlated with the fluoride emission rates and micrographs of membrane thinning published previously by Lim et al.[25]. The cumulative fluoride release from the stack measured at the end of each AST cycle is presented in Fig. 6, which indicates the overall level of chemical membrane degradation throughout the fuel cell operation. It is observed that the fluoride release rate increases until the 7th AST cycle from 0.36 µmol h^{-1} cm^{-2} to 0.85 µmol h^{-1} cm^{-2} and decreases gradually toward EOL. The fluoride release increased rapidly

due to chemical degradation and saturated at an advanced level of chemical decay that coincided with the development of significant hydrogen leaks across the membrane[25].

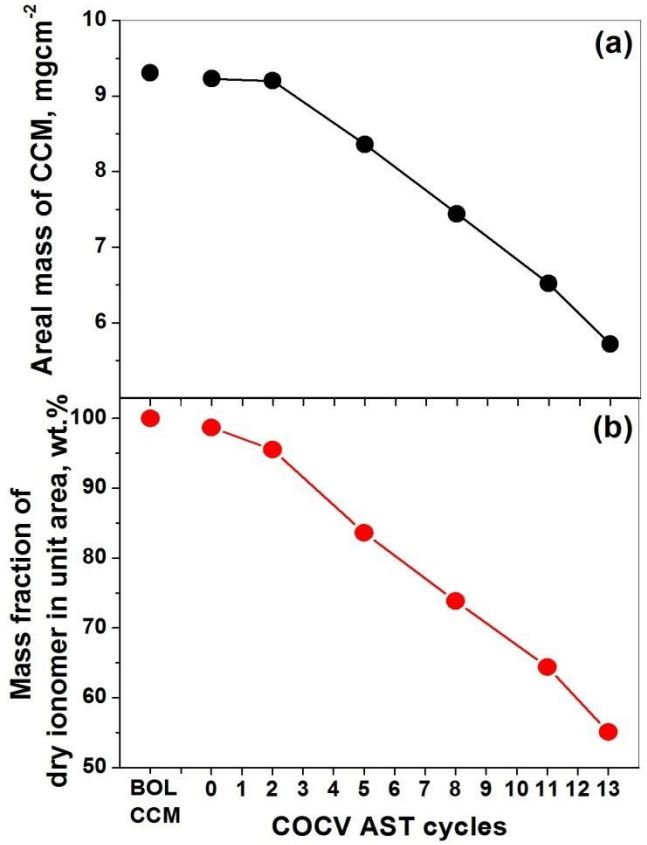

Fig. 5 (a) Areal mass and (b) remaining ionomer loading of the BOL and AST degraded CCM samples.

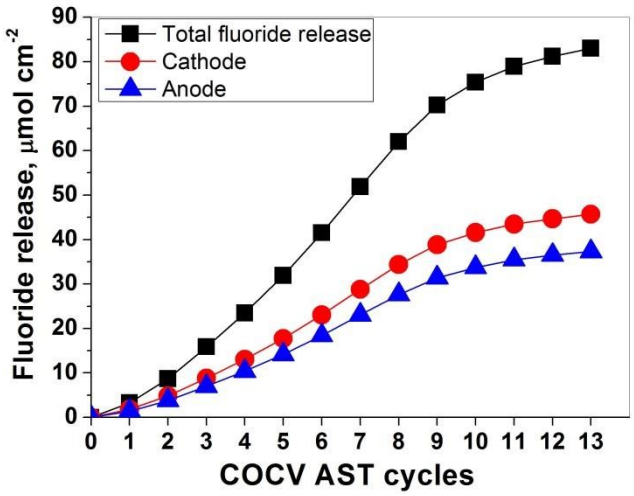

Fig. 6 Cumulative fluoride release estimated from anode and cathode effluent water, reproduced from Lim et al.[25].

Based on the information of specific gravity and thickness, the pristine membrane contained ~175 µmol cm^{-2} fluorine atoms. The membrane subjected to the AST cycles had cumulatively released ~48% of its fluorine atoms at EOL. Similarly, post AST analysis from TGA determined ~46% ionomer mass loss in the CCM. Though the loss represents the collective ionomer from the membrane and dispersed form in the catalyst layers, the major loss can be taken as the contribution from the membrane, which is in good agreement with the fluoride release data previously published[25].

3.3. Ionomer mass-normalized water uptake

The analysis of water uptake in CCMs is relatively complex due to the disparate nature of the three components and the heterogeneous structure of the catalyst layers with significant spatial variations; consequently, normalization by sample mass or planar area is somewhat ambiguous. In the context of degradation, the analysis becomes even more challenging. It is therefore proposed to normalize the CCM water uptake by ionomer mass with the aid of TGA data, provided that the majority of the water is absorbed in the ionomer in the membrane and catalyst layers. This approach is independent of spatial variations in catalyst layer structure and can accurately capture the water uptake of the membrane at various stages of degradation. The amount of ionomer phase was determined from the TGA data and the water uptake of the CCMs was normalized with respect to their dry ionomer mass. Though TGA measurements enabled determination of the mass fraction of ionomer in the CCM, the amount of ionomer in the catalyst layer and membrane were not exactly distinguished. Owing to practical ambiguities in an in-situ set up, the individual water sorption studies of degraded ionomer in the catalyst layer and membrane were not attempted.

The obtained trend in the water uptake of the ionomer in the degraded CCMs subjected to COCV AST cycles is demonstrated in Fig. 7. Theoretically, the water uptake normalized by ionomer mass should be consistent with regular water uptake measurements for pristine membranes. The BOL CCM is shown to contain approximately 30% less water per gram of ionomer than the pure membrane, which is qualitatively consistent with the area normalized water uptake data previously discussed (Fig. 3) and attributed to the physical constraint provided by the catalyst layers for membrane hygral expansion as well as the lower water sorption of the ionomer portion in the catalyst layers. A substantial increase in ionomer mass-normalized water uptake was experienced during the MEA conditioning phase and during the first two AST cycles; again, in good agreement with the area normalized data. This is anticipated due to equilibration of the membrane with water and growth of the hydrophilic domains, while only a small amount of ionomer material was lost from degradation as shown by fluoride release and ionomer TGA (Figs. 5-6). This could be qualitatively attributed to the alignment/orientation of the parallel bundles of surface ionomer structure[40]. The membrane constrained by the catalyst layers equilibrated with the carrier vapor to absorb maximum water during this time. After a few cycles, substantial loss of ionomer material occurred as a result of the high rate of chemical degradation, where significant loss of sulfonic acid functional groups was reported[25]. The water clusters in the degraded ionomer

membrane are expected to change considerably with the loss of water absorbing SO_3^- pendant chains that may disrupt the ionomer morphology and reduce the water uptake of the ionomer membrane. After the 8th cycle, the CCM water uptake per ionomer unit exhibited a sharp increase toward the EOL state. In this regime, the degradation process was dominated by mechanical degradation of chemically weakened regions and led to the development of physical damage such as cracks, voids, divots, and pinholes, which could contain a significant amount of bulk water at the fully humidified condition despite the advanced stage of chemical degradation and reduced concentration of sulfonic acid functional groups. Previously, our group reported that ~100 µm pinholes were formed at EOL at a frequency of 5 pinholes per 3 cm^2 survey area[25]. Here, it is observed experimentally that the water uptake per unit gram of ionomer increases significantly with COCV AST cycles as severe damage was formed in the membrane. This is a consequence of the combined chemical and mechanical degradation induced by the COCV AST and may not occur during purely chemical degradation. However, combined chemical and mechanical degradation is normally expected during cyclic operation of fuel cells in the field. The presence of water in the various membrane cavities (at fully humidified conditions) may be beneficial in order to reduce harmful reactant crossover and hydrogen leaks during prolonged fuel cell operation with aged membranes.

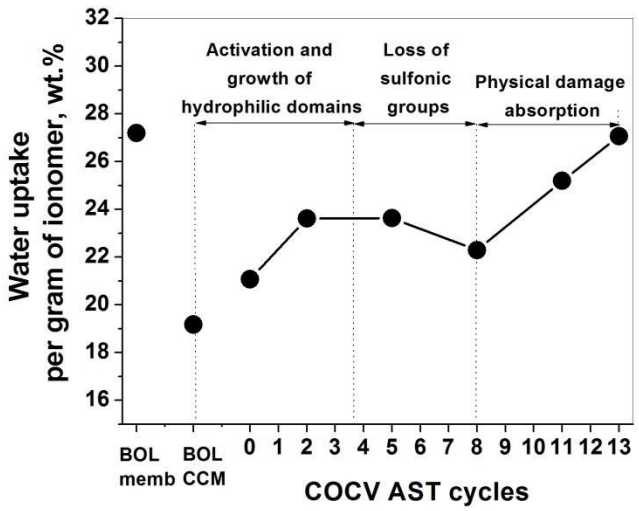

Fig. 7 Water uptake normalized by dry ionomer mass in pristine membrane, BOL CCM, and AST degraded CCMs.

3.4. Proton conductivity

In order to analyze the effects of combined chemical and mechanical degradation on the transport properties of the membrane, the proton conductivity was calculated from the in-situ measured high frequency cell impedance data[25] and illustrated in Fig. 8. The high frequency resistance (HFR) variations were small (<10%) during the degradation process, since membrane thinning and loss of proton conductivity occurred at similar rates throughout the test. After the 9th cycle, the HFR showed a marginal decrease due to the reduced rate of SO_3^- loss as the chemical degradation shifted more towards the main chain at the later stages of the test. The HFR reduction could also be due to water formation on the cathode from hydrogen leaks across the membrane that may increase the hydration of the membrane under the otherwise dry conditions of the test.

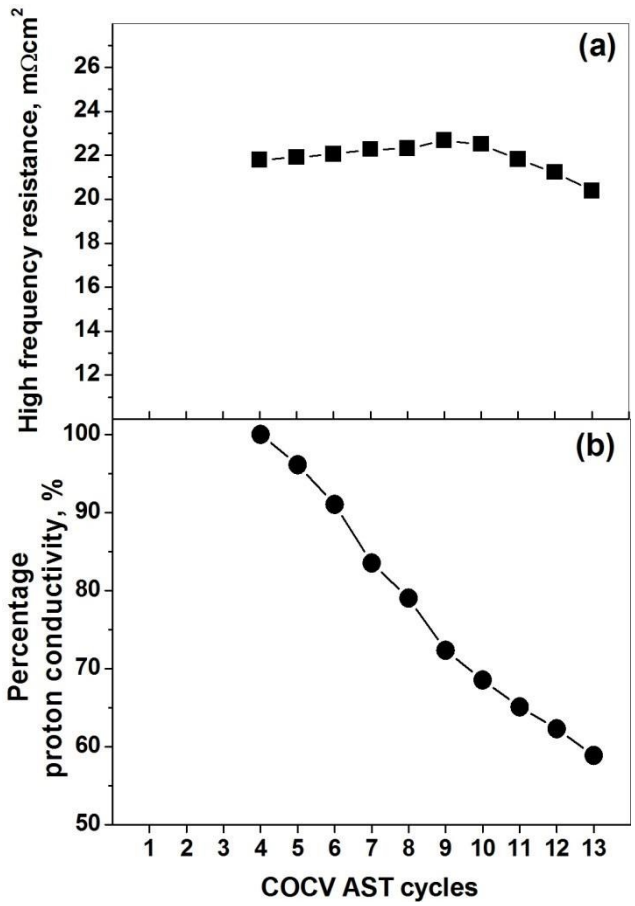

Fig. 8 (a) High frequency resistance (adopted from Lim et al.[25]) and (b) calculated proton conductivity at the end of each COCV AST cycle.

The calculated proton conductivity was found to decrease linearly with degradation, which qualitatively follows the trends observed with membrane thinning, fluoride release, and ionomer mass loss. This may also indirectly reveal that ion exchange capacity could linearly decrease during combined chemical and mechanical degradation. The proton conductivity is closely related to the acid and water content of the membrane. Notably, the observed increase in water uptake per unit gram of ionomer at the late stages of degradation did not enhance the proton conductivity of the membrane. This indicates that the additional water accumulated in the membrane did not contribute to the ionic clusters or ion-conducting water channels in the material and was rather situated in the cavities formed as a result of physical damage induced by mechanical degradation. The loss of sulfonic acid end groups through side chain degradation could be the reason

for the decreased proton conductivity despite the increasing water content.

4. Conclusions

For the first time, we report the water uptake, thermal decomposition, and ionic conductivity of in-situ degraded CCMs subjected to combined chemical and mechanical membrane degradation. We found that the water uptake of a CCM is lower than that of a pure membrane due to the constraint imposed by the catalyst layers on the hygral expansion of the membrane. However, MEA conditioning led to a considerable increase in CCM water uptake. Two normalization methods were proposed for water sorption analysis of CCMs subjected to membrane degradation: (i) normalization based on sample area, which is constant during degradation; and (ii) normalization based on ionomer mass, which accounts for the membrane thinning and mass loss caused by chemical degradation. From thermal analysis, the overall decomposition pattern of the membrane and CCM was found to be similar. Thermal analysis of in-situ degraded CCMs, however, revealed reduced thermal stability of the membrane due to chemical degradation. The mass fraction of ionomer in the degraded CCMs determined from thermogravimetric analysis was found to decrease linearly up to ~46% of the initial ionomer content due to degradation, which is commensurate with fluoride emission data. The water uptake normalized by ionomer mass increased initially due to conditioning and further slow growth of hydrophilic pores in the ionomer. Due to the degradation of hydrophilic SO_3^- bearing side chains, the water uptake decreased substantially from the 2nd cycle until the 8th cycle. At advanced stages of combined chemical and mechanical degradation, physical damage such as cracks and pinholes attracted more water in cavities near the membrane end-of-life. This sharp increase in water uptake per ionomer unit did not enhance the proton conductivity of the membrane; in contrast, the proton conductivity decreased linearly, indicating that the water residing in damage cavities does not contribute to ion conduction. However, the fact that the membrane cavities are filled with water during fully humidified conditions can be beneficial in order to reduce reactant gas crossover and hydrogen leaks during fuel cell operation with aged membranes.

In summary, these findings improve the fundamental understanding of water uptake in degraded membranes and can contribute to bridging the existing gap between ex-situ water uptake studies and in-situ fuel cell testing. The present results are particularly relevant for understanding the complex effects of combined chemical and mechanical membrane degradation and how to manage such effects during field operation of fuel cells. The time dependent molecular structure of the ionomer with degradation and its correlation to changes in water sorption and transport properties may also be useful for the development of degradation and durability models for fuel cell stacks.

Acknowledgements

Funding for this research provided by Automotive Partnership Canada (APC), Natural Sciences and Engineering Research Council of Canada (NSERC), and Ballard Power Systems is gratefully acknowledged. Ballard Power Systems is also acknowledged for providing material samples, access to experimental facilities, and technical support. The authors gratefully acknowledge Xiaoyan Luo, Marc-Antoni Goulet, Timothy J. Peckham, and Lida Ghassemzadeh for insightful technical discussions.

Notes and references

[a] School of Mechatronic Systems Engineering, Simon Fraser University, 250-13450 102 Avenue, Surrey, BC V3T0A3, Canada. E-mail: ekjeang@sfu.ca; Tel: +1 778 782 8791; Fax: +1 778 782 7514

[b] Ballard Power Systems, 9000 Glenlyon Parkway, Burnaby, BC V5J5J8, Canada.

[c] Department of Chemistry, Simon Fraser University, 8888 University Drive, Burnaby, BC V5A1S6, Canada.

1 T.A. Zawodzinski, C. Derouin, S. Radzinski, R.J. Sherman, V.T. Smith, T.E. Springer, and S. Gottesfeld, *J. Electrochem. Soc*., 1993, **140**, 1041-1047.
2 S. Slade, S.A. Campbell, T.R. Ralph, and F.C. Walsh, *J. Electrochem. Soc.*, 2002, **149**, A1556-A1564.
3 M.P. Rodgers, Z. Shi, and S. Holdcroft, *J. Membr. Sci*., 2008, **325**, 346-356.
4 K.T. Adjemian, R. Dominey, L. Krishnan, H. Ota, P. Majsztrik, T. Zhang, J. Mann, et al., *Chem. Mater.*, 2006, **18**, 2238-2248.
5 S. Venkatesan, V. Guruviah, N. Hebalkar, and K.S. Dhathathreyan., *Int. J. Hydrogen Energy*, 2011, **36**, 14815-14822.
6 Z. Qi, and A. Kaufman, *J. Power Sources*, 2002, **109**, 38-46.
7 J. Chen, T. Matsuura, and M. Hori, *J. Power Sources*, 2004, **131**, 155-161.
8 P. Majsztrik, M. B. Satterfield, A. Bocarsly, and J. Benziger, *J. Membr. Sci.*, 2007, **301**, 93-106.
9 M.J. Cheah, I.G. Kevrekidis, and J. Benziger, *J. Phys. Chem. B*, 2011, **115** (34), 10239–10250.
10 B. Kientiz, Y. Haruhiko, N. Nobuaki, and A.Z. Weber, *J. Fuel Cell Sci. Technol*., 2010, **8**(1), 011013.
11 M. Adachi, Z. Shi, T. Navessin, and S. Holdcroft, *J. Electrochem. Soc.*, 2009, **156**, B782-B790.
12 G.S. Hwang, M. Kaviany, J. T. Gostick, B. Kientiz, A.Z. Weber, and M.H. Kim, *Polymer*, 2011, **52**, 2584-2593.
13 J. Benziger, A. Bocarsly, M.J. Cheah, P. Majsztrik, B. Satterfield, and Q. Zhao, in Fuel Cells and Hydrogen Storage 141, Bocarsly and Mingos, Editors, p. 85, Springer, Berlin Heidelberg 141 (2011).
14 Y. Yang, A. Siu, T.J. Peckham, and S. Holdcroft, in Advances in Polymer Sciences 215: Fuel cells 1, G.G. Scherer, Editor, p. 55, Springer, Berlin Heidelberg 215 (2008).
15 M.B. Satterfield, and J. Benziger, *J. Polym. Sci., Part B: Polym. Phy.*, 2009, **47**, 11-24.
16 R. Hiesgen, S. Helmly, T. Morawietz, X-Z. Yuan, H. Wang, and K.A. Friedrich, *Electrochim. Acta*, 2013, **110**, 292-305.
17 L. Ghassemzadeh and S. Holdcroft, *J. Am. Chem. Soc*., 2013, **135**, 8181-8184.
18 D.E. Moilanen, I.R. Piletic, and M.D. Fayer, *J. Phys. Chem. A*, 2006, **110**, 9084-9088.
19 M. Danilczuk, L. Lancucki, S. Schlick, S.J. Hamrock, and G.M. Haugen, *ACS Macro Lett.*, 2012, **1**, 280-285.
20 K.H. Wong, and E. Kjeang, *J. Electrochem. Soc.*, 2014, **161**, F823-F832.
21 K.H. Wong, and E. Kjeang, *ChemSusChem.* 2015, DOI: 10.1002/cssc.201402957.
22 R.M.H. Khorasany, E. Kjeang, G.G. Wang, and R.K.N.D. Rajapakse, *J. Power Sources*, 2015, **279**, 55-63.
23 R.M.H. Khorasany, A. Sadeghi Alavijeh, E. Kjeang, G.G. Wang, and R.K.N.D. Rajapakse, *J. Power Sources*, 2015, **274**, 1208-1216.
24 A. Kusoglu, M. Calabrese, A.Z. Weber, *ECS Electrochem. Lett.* 2014, **3(5)**, F33-F36

25 C. Lim, L. Ghassemzadeh, F. Van Hove, M. Lauritzen, J. Kolodziej, G.G. Wang, S. Holdcroft, and E. Kjeang, *J. Power Sources*, 2014, **257**, 102-110.
26 A. Sadeghi Alavijeh, M.-A. Goulet, R.M.H. Khorasany, J. Ghataurah, C. Lim, M. Lauritzen, E. Kjeang, G.G. Wang, R.K.N.D. Rajapakse, *Fuel cells*, 2015, **15**, 204–213.
27 L. Ghassemzadeh, T. J. Peckham, T.Weissbach, X. Luo, and S. Holdcroft. *J. Am. Chem. Soc*., 2013, **135**, 15923-15932.
28 S. Mu, C.Xu, Q. Yuan, Y. Gao, F. Xu, and P. Zhao, *J.App. Polym. Sci.*, 2013 **129**, 1586-1592.
29 M-A. Goulet, R.M.H. Khorasany, C.D. Torres, M. Lauritzen, E. Kjeang, G.G. Wang, and R.K.N.D. Rajapakse, *J. Power Sources*, 2013, **234**, 38-47.
30 M-A. Goulet, S. Arbour, M. Lauritzen, and E. Kjeang, *J. Power Sources*, 2015, **274**, 94-100.
31 R.M.H. Khorasany, M-A. Goulet, A. Sadeghi Alavijeh, E. Kjeang, G.G. Wang, and R.K.N.D. Rajapakse, *J. Power Sources*, 2014, **252**, 176-188.
32 S. Ge, X. Li, B. Yi, and I-M. Hsing, *J. Electrochem. Soc*., 2005, **152**, A1149-A1157.
33 S. Holdcroft, *Chem. Mater*., 2013, **26**, 381-393.
34 T. Soboleva, K.Malek, Z. Xie, T. Navessin, and S. Holdcroft, *ACS Appl. Mater. Interfaces*, 2011, **3(6)** 1827-37.
35 V. Berejnov, D. Susac, J. Stumper, and A.P. Hitchcock., *ECS Trans.*, 2011, **41**, 395-402.
36 H.P. Gunterman, A. Kwong, J.T. Gostick, A. Kusoglu, and A.Z. Weber, *ECS Trans.* 2011, **41**, 647-650.
37 S. Venkatesan, V. Guruviah, R. Natarajan, and K.S. Dhathathreyan, *Int. J. Hydrogen Energy*, 2014, **39**, 1752-1759.
38 S.H. De Almeida, Y.J. Kawano, *Therm. Anal. Calorimet.* 1999, **58**, 569-577.
39 S.R. Samms, S. Wasmus, and R.F. Savinell, *J. Electrochem. Soc*., 1996, **143**, 1498-1504.
40 K-D. Kreuer, *Solid State Ionics*, 2013, **252**, 93-101.

